https://doi.org/10.1142/9789811278952_0017

Chapter 17

Vacuum System

Vincent Baglin, Paolo Chiggiato and Cedric Garion

CERN, TE Department, Geneva 23, CH-1211, Switzerland

The HL-LHC project requires an important upgrade of the LHC vacuum system to ensure sufficient beam lifetime, limit the background to the high-luminosity experiments, protect the new final focusing system from ionizing radiation, increase the mechanical robustness, maximize beam aperture and mitigate electron multipacting. The technologies developed to tackle these challenges are exposed in this chapter.

1. Introduction

In the beam vacuum chambers of the Large Hadron Collider (LHC), two beams circulate in opposite direction in a 27 km circumference tunnel about 100 m underground [1, 2]. 'Two-in-one' superconducting magnets are cooled down with superfluid helium at 1.9 K. They provide the required magnetic field to maintain the hadron beams on a stable orbit during acceleration, from 450 GeV to collision energy, and during physics operation. In a bent trajectory, charged particles at relativistic speed emit synchrotron radiation. In the LHC at nominal energy and intensity, i.e. 7 TeV and 0.58 A, the two proton beams emit 8 kW of synchrotron radiation power, mostly in the 8.33 T superconducting bending magnets. Synchrotron radiation results in stimulated molecular desorption from the vacuum chamber walls and in the transfer of energy to the cryogenic system. To avoid an excessive cooling power, a so-called 'beam screen' is inserted into the magnets' cold bore. Its main role is intercepting the heat load at a higher temperature than 1.9 K, namely in the 5-20 K range.

Perforations made on the top and bottom of the beam screen provide pumping of the desorbed molecules on the cold bore. Perforations are such to produce a beam-screen transparency of 4.4% which ensures a beam vacuum lifetime longer than 100 h, well above the beam lifetime given by proton burn-off rate. These perforations limit also the heat load to the cold masses, due to proton scattering on the residual gas, at an acceptable level below 80 mW/m [3].

In the LHC experiments, ~30 000 Higgs particles are produced per year to study in detail the Standard Model and scrutinize the appearance of new physics beyond the Standard Model. This physics goal requires a luminosity as high as 1×10^{34} $s^{-1}\times cm^{-2}$ obtained by the focalization of dense proton bunches at the collision point. Despite the fact that most of the fragments produced at the collision point are intercepted by the experimental detector, there is a significant fraction of the collision debris, emitted at small angle, which escapes towards the storage ring. Indeed, from the beginning of the LHC project, it was anticipated that the large amount of debris would lead eventually to the damage of the superconducting final focusing quadrupoles located 20 to 60 m away from the collision point. Since the preliminary study for an upgrade in luminosity of the LHC, a tungsten shielded beam screen was proposed in order to mitigate the cold mass damage and heat load [4]. The insertion of tungsten in the space between the beam screen and the cold bore required a larger bore aperture provided by the new superconducting quadrupoles based on Nb_3Sn technology. Since then, the conceptual design has evolved to become a cornerstone of the upgraded vacuum system for the High Luminosity LHC (HL-LHC) [5].

The next sections will present the scientific and technological developments that build the foundation of the HL-LHC vacuum system. To this aim, we discuss in detail the performance requirements, the new HL-LHC beam screen, the new anti-multipacting surface treatment to mitigate the electron cloud build-up, a potential showstopper of the upgrade, and the modifications of the vacuum layout.

2. Performance Requirements

The HL-LHC upgrade will increase by one order of magnitude the LHC integrated luminosity with the objective to provide about 3 000 (and ulti-

mately 4 000) fb^{-1} by around 2040. To do so, the instantaneous luminosity will be leveled at 5×10^{34} $s^{-1}\times cm^{-2}$ to maintain the number of events per bunch crossing at an acceptable value (~130) for the experimental detectors. Special transversely deflecting RF cavities RF (so-called 'crab cavities', see Chapter 7) rotate the proton bunches to increase the virtual luminosity beyond 10^{34} $s^{-1}\times cm^{-2}$ and dynamic beta* with crossing angle adjustments are used to compensate the proton burn-off during the collisions and to keep the collision rate levelled at 5×10^{34} $s^{-1}\times cm^{-2}$. The required beta* range will be attained thanks to a novel optic concept: the Achromatic Telescopic Squeeze (ATS). This concept is possible thanks to the large beam aperture available in the LHC arcs to pre-squeeze the beam and use the matching quadrupoles of the neighboring insertions to perform a final telescopic squeeze. The ATS allows to reach a much lower beam size at the collision point (β^*) for a larger proton density ($\gamma \times n_b \times N_b^2 / \varepsilon_n$) than the one of LHC, see Table 1 and Chapter 5.

The HL-LHC vacuum system shall be upgraded to cope with the increased luminosity, beam intensity and bunch population. In order to face the higher beam intensities, the vacuum beam lifetime shall be doubled with respect to LHC, thus increased to 200 h, requiring approximately half the gas density in the beam vacuum system to maintain the beam-gas losses on the cold mass below 80 mW/m. Table 2 gives for both machines the maximum number density for single gas species usually found in vacuum systems. Low mass molecules (H_2) are less critical than heavy molecules (CO_2) that have larger beam-gas cross sections.

Table 1. LHC and HL-LHC nominal beam parameters.

		LHC	HL-LHC
Energy	TeV	7	7
Luminosity (ultimate)	$\times10^{34}$ $s^{-1}\times cm^2$	1 (2.3)	5 (7.5)
Intensity	A	0.58	1.1
Number of bunches, n_b		2808	2760
Proton per bunches, N_b	$\times10^{11}$	1.15	2.2
Bunch spacing	ns	25	25
β^*	cm	55	55-15
Normalized emittance, ε_n	μm	3.75	2.2
Events/crossing (ultimate)		27 (62)	131 (200)

Table 2. LHC and HL-LHC maximum acceptable number densities (m^{-3}) for single gas.

	H_2	CH_4	H_2O	CO	CO_2
LHC	1.2×10^{15}	1.8×10^{14}	1.8×10^{14}	1.2×10^{14}	7.9×10^{13}
HL-LHC	6.4×10^{14}	9.6×10^{13}	9.6×10^{13}	6.4×10^{13}	4.2×10^{13}

Table 3. Acceptable H_2 equivalent number densities (m^{-3}) in the LHC and HL-LHC experiments and IRs.

	ATLAS	CMS	IR1&5	IR2&8
LHC	1.5×10^{11}	3.1×10^{12}	5.3×10^{12}	6.5×10^{12}
HL-LHC	8.0×10^{10}	1.6×10^{12}	2.8×10^{12}	3.5×10^{12}

Similarly, the background to the LHC experiments due to beam-gas scattering in the interaction regions (IR) and inside the experimental beam pipes must be acceptable for the physics run. Table 3 gives the tolerable H_2 equivalent gas density, scaled with the beam intensity, for the LHC and HL-LHC high-luminosity experiments. As shown, the IR1 & IR5, where most of the HL-LHC upgrade is taking place, shall be designed to achieve an averaged H_2 equivalent gas density of 2.8×10^{12} H_2 equiv/m^3. This value corresponds to a pressure of 1×10^{-10} mbar assuming only hydrogen in the vacuum system. In the IR, the required pressure is mainly defined by the requirements of the cryo-elements and beam equipment deserving a specific attention, such as collimators, masks, etc.

3. Shielded Beam Screen

The major modification of the LHC vacuum system is taking place in the final focusing system, so-called Inner Triplet (IT), where a beam screen equipped with a tungsten alloy shielding is inserted into the cold bore to protect the cold mass from unduly deterioration due to radiation and excessive beam induced heat load (see Chapter 15) [6].

The shielded beam screen is installed along ~60 m. It starts at 22.5 m from the interaction point (IP) and extends inside the quadrupoles Q1, Q2, Q3, the corrector package (CP) and the dipole D1 that are all housed in a single vacuum vessel made of 6 cryostats. Two types of shielded beam screens with unit length in the range 8-11 m will be produced and inserted in a seamless 4 mm thick 316LN cold bore tube of 136.7 mm inner diameter. Most of the debris escaping the cavern through the 60 mm diameter sec-

ondary absorber (named TAXS) are intercepted by Q1. For that reason, the tungsten shielding is thicker in that position, i.e. 16 mm. The thickness is reduced to 6 mm in the other magnets located downstream of Q1. Such reduction ensures the larger aperture required in the Q2 magnet.

As shown in Figure 1, the shields are placed in the vertical and horizontal plane to intercept the charged particles debris produced at the interaction point emitted towards the cold mass in a plane depending on the crossing angle configuration. The absorbed power ranges from 15 W/m to 25 W/m at Q1. The 40 cm long absorber blocks are positioned on the beam screen tubes by pins, and they are hold in place by Ti elastic rings.

Similar to the LHC, the gas pumping towards the 1.9 K cold bore is granted by longitudinal slots punched in the beam screen shell. The transparency is set to 2% providing a total perforated area of 60 cm^2/m. The perforations are located at the magnet's pole. For this reason, to protect the cold bore from direct impingement of electrons or scattered photons, electron shields are placed above the slots and clipped on the cooling tubes. The resulting pumping speed, computed by Monte-Carlo with Molflow, equals 430 ℓ/s per meter of beam screen for nitrogen at 20 °C, i.e. 15% more than in the LHC arcs.

Four 10-mm-diameter cooling tubes are laser welded on the external side of the beam screen tube. The heat load deposited on the tungsten absorbers

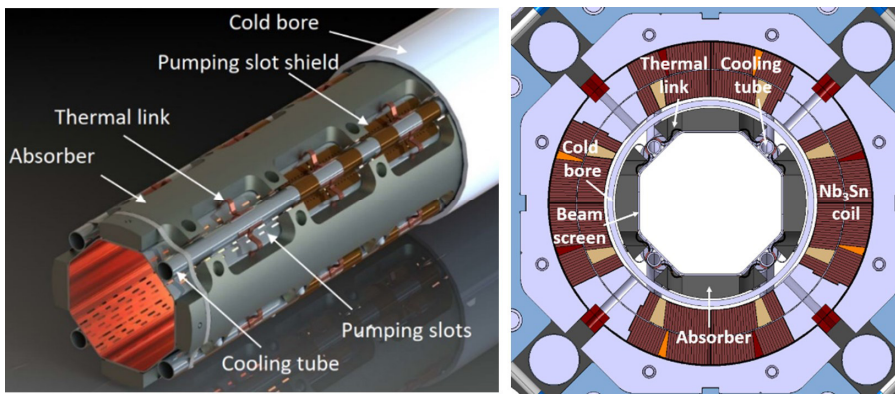

Fig. 1. Left, the Q1 shielded beam screen inserted in its cold bore tube (for illustration, one electron shield has been removed to show the slots behind); Right, cross-section of the Q1 cold mass.

is transferred to pressurized gaseous helium by Cu thermal links directly connected to the cooling tube. This thermal design has been thoroughly simulated and experimentally validated by a 1-m-long laboratory mock-up [7, 8]. The thermal links ensure a stable operating temperature of the beam screen from 60 to 80 K along the cryostat.

The beam screen aperture is maximized to provide sufficient operational margin for the beam optics. The chosen geometry of the aperture is an octagon with 99.7 mm distance between diametrically opposed faces for Q1, and 119.7 mm in horizontal/vertical plane and 110.7 mm in the 45° plane for the other magnets.

As for the LHC, the beam screen is made of Cu-colaminated high-Mn high-N austenitic stainless steel (P506). The ~75 μm thick Cu layer provides an electrical resistivity of around 2.10^{-9} Ω.m at operating temperature, which complies with the beam impedance budget. The P506 steel provides structural robustness in the event of transitions from the superconducting to resistive state of the magnet cables (*i.e.* a 'quench'). In such events, large forces are induced by the Foucault currents circulating in the Cu layer. These currents induce also torques and forces in the tungsten absorbers, which are designed accordingly.

An elastic supporting system using ceramic (ZrO_2) balls and Ti springs is used to support the shielded beam screen in the cold bore. Such design solution limits the heat transfer by conduction from the beam screen to the cold bore and facilitates the insertion of the ~500 kg shielded beam screen into the cold bore. In the occurrence of a magnet quench, the supporting system can retract and the deformed beam screen, designed to be elastic, goes in contact with the cold bore tube. In such a way, the forces due to the induced currents are homogenously redistributed. The maximum contact force between the tungsten blocks and the cold bore is around 350 N/mm.

This mechanical design has been carefully simulated and validated in the laboratory. 2-m-long beam screen underwent a sequence of ~50 quenches during the prototyping phase of the HL-LHC quadrupole magnets up to 18.2 kA [9].

Between cold masses, the beam screen is interrupted, and the beam vacuum line is connected with an upgraded interconnecting system that includes tungsten shielding and a deformable RF bridge that provided continuity for the images currents (with both a DC and an RF components).

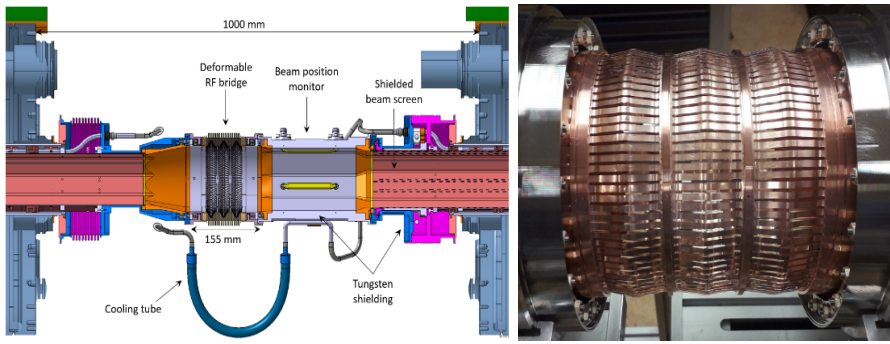

Fig. 2. Left, the HL-LHC interconnection; Right, picture of the deformable RF bridge in working position (courtesy of J. Perez Espinos, CERN).

As shown in Figure 2, the 1-m-long interconnection ensures a transition from octagonal to circular shape. It integrates a shielded beam position monitor, a cold mass shielding and a deformable RF bridge. The tungsten shielding reduces further the cold mass irradiation by the collision debris. The new RF bridge is based on a completely new design with respect to the LHC and consists of a set of V-shape convolutions manufactured from a flexible and deformable thin-walled Cu-Be element. It is produced with a single component and, consequently, it is more robust than conventional sliding RF fingers based on two independent pieces, like the LHC RF bridge. By this design feature, the risk of having an RF finger protruding into the beam aperture is eliminated [10]. In addition to the longitudinal movement, the new RF Bridge allows a transversal offset of up to 5 mm.

4. Anti-multipacting Surface Treatment

Another major upgrade of the LHC vacuum system is the introduction of an anti-multipacting surface treatment to mitigate electron cloud build-up (see Chapter 5). This phenomenon, which limits high-intensity positive-charged beam accelerators, is mainly driven by the emission of secondary electrons from the surface wall under primary electron impact.

In the LHC cryo-elements and some room temperature equipment (collimators, kickers etc.), the secondary electron yield (SEY) of the surfaces exposed to the beam is reduced by electron bombardment; this process is

called 'beam scrubbing'. The maximum SEY, δ_{max}, of fully scrubbed surfaces is expected to reach a value between 1.2 and 1.4, depending on the machine position and/or surface state [11, 12]. The remaining part of the LHC vacuum chambers (room temperature pipes, experimental areas) relies on a Non-Evaporable Getter (NEG) thin film that strongly mitigates the electron cloud build up (since $\delta_{max} \sim 1.1$) while offering pumping speeds as large as ~1 000 ℓ/s for hydrogen at 20 °C per meter of 8-cm diameter tube.

In the HL-LHC, with the advent of more intense bunch current, the electron cloud induced heat load will no longer be negligible for the IT beam screen, even with a fully scrubbed surface. Indeed, since in these magnets the beams circulate in opposite directions, the heat load may be as large as 500-1100 W (against 250-500 W at present for LHC) [13]. Moreover, the electron conditioning efficiency is strongly dependent on the electron cloud activity and surface state. To achieve a rapid commissioning of the HL-LHC vacuum system without dedicated and unpredictable "scrubbing runs", a pre-treatment of the cryo-element's beam screen surface is highly desirable to mitigate the electron cloud. The target of the treatment is reducing δ_{max} down to or below one. The base line treatment is amorphous carbon (a-C) thin film coating, successfully deployed in the CERN SPS to mitigate electron cloud build-up. An alternative solution based on laser surface treatment is also under study and development [14, 15, 16].

The performance of the a-C coating was evaluated meticulously at cryogenic and room temperatures. In particular, adsorption isotherms, secondary electron and photon stimulated desorption yields were measured in the laboratory. The anti-multipacting behavior of the a-C coating was demonstrated with a mock-up installed in the SPS ring.

Adsorption isotherm measurements showed that the coating is porous (~300 times the Cu monolayer capacity). The high porosity is beneficial to reduce the secondary electron yield. However, at cryogenic temperatures, it amplifies the quantity of physisorbed molecules, in particular hydrogen up to ~60 K. For temperatures higher than 60 K, most of the physisorbed hydrogen is released. For this reason, the operating temperature of the a-C coated beam screen was set to be 60 to 80 K.

Studies with synchrotron radiation at grazing incidence with critical energy ranging from 10 to 1 000 eV were done. They revealed that the photon stimulated molecular desorption yield of a-C thin films at room

temperature is very similar to the one of oxygen-free Cu, which had allowed to define the beam screen transparency.

Finally, a demonstration of the electron multipacting suppression at crygenic temperature was realised using the COLDEX experimental set-up in SPS that mimics a beam screen / cold bore assembly. In 2015-2016, several studies with a ~500 nm thick a-C coating were held during scrubbing runs and dedicated machine development periods. These studies included measurements at different temperatures 10, 20, 50, 60 K with and without pre-condensed gas (H_2, CO, CO_2) onto the surface. The experimental results, supported by theoretical expectations derived from the PyCloud simulation code, demonstrated the absence, for LHC beams, of electron multipacting in an a-C coated beam screen with 67 mm inner diameter, located in a magnetic field free environment [17].

Figure 3 exhibits the simulated electron activity expected in the COLDEX set-up as a function of the maximum SEY. The absence of electron signal above the detection limit (10^{-10} A), together with the absence of pressure increase (larger than10^{-10} mbar), demonstrated the anti-multipacting property of the material and showed that the maximum SEY is below 1.1 at cryogenic temperatures [18]. The measurement was performed with LHC beams in the SPS.

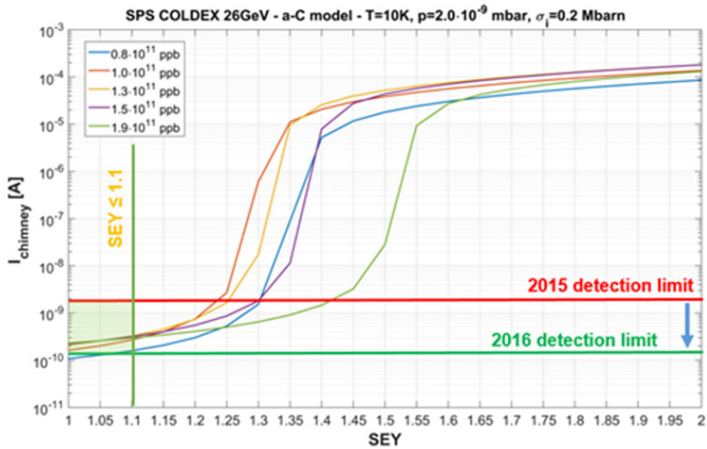

Fig. 3. Evaluation of the maximum secondary electron yield of the a-C coating from the electron activity measured with the COLDEX set-up (Courtesy R. Salemme). Figure 11-34 in [18].

The HL-LHC project foresees the modification of the IT in IR1 and IR5 that will house the a-C coated shielded beam screens. However, the triplets around IP2 and IP8 also require a specific surface treatment to reduce the beam induced heat load on the beam screen to an acceptable value. The solution chosen here was also a coating of the beam screens with a-C. Indeed, the coating technique is less expensive and less invasive than a modification of the cryogenic cooling system.

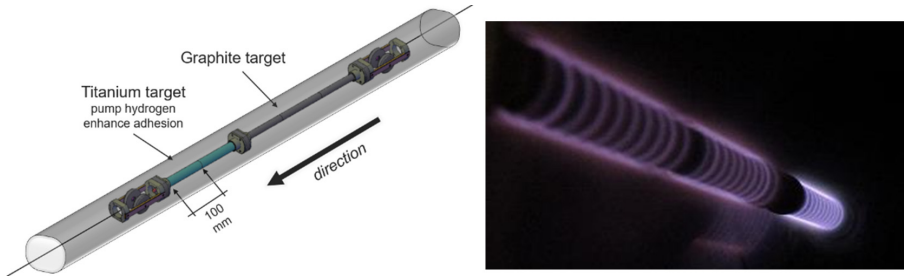

Fig. 4. Left, modular sputtering source for the in-situ coating of the LHC triplets in IR2 and 8; Right, glow discharge during the coating process (courtesy P. Costa Pinto, CERN) [14].

In order to avoid the complete dismounting of the triplets in IP2 and IP8 for the treatment, an innovative solution was worked out to perform an in-situ carbon coating by sputtering using graphite cathodes in an Ar plasma. As shown in Figure 4, a modular sputtering source, made of 100 mm long elements assembled together, was developed to allow the insertion in the tiny space left when the plug-in-modules are removed from the triplets' interconnects. The source is made of a Ti and a graphite target. The former is required to perform a pre-coating of the same material. The purpose of the Ti film is pumping H_2 during the process and enhancing the C adhesion; the removal of H_2 from the plasma is essential to achieve maximum SEY below one. Remotely controlled spools are actuated to move the targets and power the material sputtering. The whole process results in ~100 nm of Ti underlayer onto which is deposited a ~50-100 nm C layer mixed with a ~150 nm Ti layer. When needed, preliminary etching of oxidized Cu surfaces may be provided by Ar inverted sputtering.

This approach will be used also for the a-C coating of a few other standalone magnets in the long straight sections 2 right and 8 left for the sake of

re-equilibrating the available cooling power around the LHC ring. The technique may be ultimately used also to mitigate the electron cloud build-up in the LHC arcs since, more than 15 years ago, the storage ring was not designed to operate with the HL-LHC beam.

More recently, significant collaborative efforts have been made to develop further the laser treatment of surface [16]. This technology offers the advantage to treat the material under inert atmosphere thereby simplifies the production. As shown in Figure 5, the laser ablation produces a blackened Cu surface with grooves and microstructures that results to SEY well below 1.

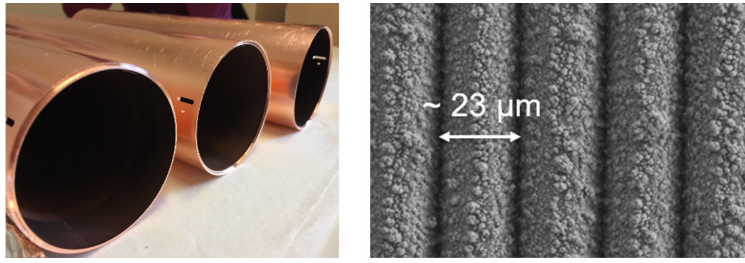

Fig. 5. Left, laser treated surface; Right, microscope view of the laser treated surface (courtesy A.T. Perez Fontenla, CERN) [17].

Beside the technical challenge to produce a mole capable of treating meters of vacuum tube, the large parameter space intrinsic to this technology, must be also studied to select the appropriate parameters compatible with the accelerator needs. As such, the behavior at cryogenic temperature during beam circulation, the surface impedance and the vacuum properties of the laser treated surface are still under intense investigation. However, the results obtained so far are very promising for a future implementation.

5. Vacuum Layout

An additional upgrade of the LHC vacuum system concerns the instrumentation of the experimental beam pipes. The experimental beam pipes are designed to be as much as possible transparent to the products of interaction and have an overall volume as small as possible to position the detectors as close as possible around the vertex. For these reasons, during the LHC design, the vacuum instrumentation was deported outside the experimental

cavern in the LHC tunnel between the secondary absorber and the first quadrupole of the IT, namely Q1.

However, during maintenance periods, this location poses important issues of safety for the personnel linked to oxygen deficiency and radiation hazards. Therefore, the HL-LHC design foresees the installation of these vacuum instruments in the experimental cavern at each extremity of the ~30 m long experimental beam pipe (see Chapter 13) [19]. This new layout solves not only the safety issue but, additionally, allows to install the first quadrupole, Q1, at 22.5 m from the IP, closer than in LHC (23 m), for a better beam squeeze.

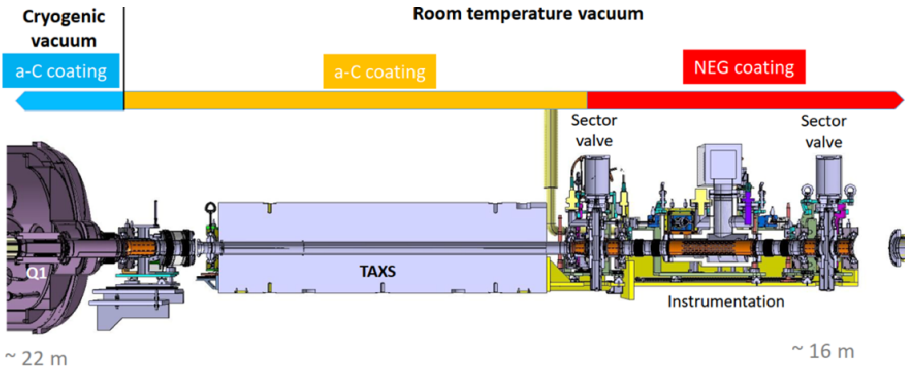

Fig. 6. The remotely connectable/disconnectable vacuum instrumentation and sector valves modules of the HL-LHC high luminosity experiments (courtesy J. Perez-Espinos).

Figure 6 shows the HL-LHC vacuum layout from Q1 to 16 m from the IP where the vacuum instrumentation for the high luminosity experiments is located. The system is made of three modules that can be independently and remotely connected/disconnected. During maintenance periods, a double valve sectorisation ensures a full decoupling between the experimental beam pipe and the triplets.

The TAXS, which separates the experimental cavern from the accelerator tunnel, is operated at room temperature with its 60-mm-diameter copper tube, which is coated with a-C. Q1 is operated at cryogenic temperature and its beam screen is carbon coated as well. Both systems are unbaked.

Similarly to the LHC, the remaining part of the long-straight-section vacuum system, including the experimental beam pipe, is coated with NEG

thin film that needs to be activated at ~200 °C to achieve the required pumping speed and low SEY required for the machine operation.

A last upgrade of the HL-LHC vacuum system is the implementation of a Full Remote Alignment system (FRAS), see Chapter 22, which aims to compensate the experimental cavern movements and local misalignments without intervention in the tunnel. That remote action will minimize the radiation dose to the personnel and allows more frequent alignment campaign which favors in turn to reduce the aperture margins in these locations.

The HL-LHC vacuum system layout is conceived to cope with the new remote alignment. When possible, it provides a large enough aperture to avoid component's re-alignment, deformable RF bridges to handle large transverse offset (>2.5 mm) and FRAS' supporting tables for components that require regular alignment.

The remaining part of the vacuum layout is based on the LHC design that has proven to guarantee reliable machine performance. In particular, a sector valve decouples cryogenic from room temperature vacuum sectors. The separation allows NEG activation without contamination of the cryogenic part and warming the cold part without saturating the NEG coating [2].

6. Conclusions

The HL-LHC upgrade is a major intervention on more than 1.2 km of the LHC ring. It requires an upgrade of the vacuum system and the development of new technologies to cope with the luminosity increase.

An innovative beam screen, operating at cryogenic temperature, that includes shielding and an anti-multipacting surface treatment, while maximizing the beam aperture, is one of the pillars of the upgrade. The development of an in-situ coating technology, based on a modular Ti-C sputtering target, will mitigate the electron cloud build up where required. Finally, the optimization of the vacuum system instrumentation, in particular near the high-luminosity experiments, will facilitate the maintenance of the system and limit the radiation exposure to the personnel.

The vacuum system upgrade presented here is developed and tested during 10 years to allow study, design, prototyping, construction and installation, by 2026-28, for a machine start scheduled in 2029. As for the LHC, the vacuum systems and subsystems are to be thoroughly tested in the

laboratories and accelerators. This approach ensures a proper performance of the vacuum system for the future HL-LHC. There is no doubt that most of the innovative technologies discussed above will trigger future developments for the post-LHC colliders.

Acknowledgments

The LHC vacuum system upgrade for the HL-LHC implementation is the result of team work of many colleagues, associates and collaborators of the vacuum, surfaces & coatings group. All of them deserve special recognition.

References

1. L. Evans, Ed, The Large Hadron Collider: a Marvel of Technology, EPFL Press.
2. O. Brüning, P. Collier, P. Lebrun, S. Myers, R. Ostojic, J. Poole, P. Proudlock Eds. LHC Design Report, Vol 1 The LHC Main Ring, CERN-2004-003, 2004.
3. O. Gröbner, Overview of the LHC vacuum system, *Vacuum* 60 (2001) 25-34.
4. R. Ostojic, L. Williams Eds, Conceptual Design of the LHC Interaction Region Upgrade – Phase-I, LHC Project Report 1163, CERN, 2008.
5. G. Apollinari, I. Béjar Alonso, O. Brüning, P. Fessia, M. Lamont, L. Rossi, L. Tavian Eds, High-Luminosity Large Hadron Collider (HL-LHC) Technical Design Report V.0.1, CERN-2017-007-M.
6. V. Baglin, C. Garion, R. Kersevan, Preliminary design of the High-Luminosity LHC beam screen with shielding, In *Proc. 6th International Particle Accelerator Conference*, IPAC 2015, pp 60-63, Richmond, VA, USA (May 2015).
7. C. Garion et al, Material characterisation and preliminary mechanical design for the HL-LHC shielded beam screens operating at cryogenic temperature, 2015 *IOP Conf. Ser.: Mater. Sci. Eng.* **102** 012013.
8. P. Borges de Sousa et al, Parametric study on the thermal performance of beam screen samples of the High-Luminosity LHC upgrade, 2017 *IOP Conf. Ser.: Mater. Sci. Eng.* **278** 012053.
9. M. Morrone, Thermomechanical study of complex structure in the aperture of superconducting magnets: application to the design of the High-Luminosity LHC shielded beam screen, *PhD: Imperial Coll.*, *London: 2018-01-31*, CERN-THESIS-2018-052.
10. J. Perez-Espinos, C. Garion, Analysing and testing of a new RF bridge concept as an alternative to conventional sliding RF fingers in LHC, In *Proc. 7th International Particle Accelerator Conference*, IPAC 2016, pp 3660-3662, Busan, Korea (May 2016).
11. V. Baglin, The LHC vacuum system: Commissioning up to nominal luminosity, *Vacuum* 138 (2017) 112-119.

12. P. Dijkstal, G. Iadarola, L. Mether, G. Rumolo, Simulation studies on the electron cloud build-up in the elements of the LHC arcs at 6.5 TeV, CERN-ACC-Note-2017-0057, CERN, Geneva, Switzerland (October 2017).
13. G. Skripa and G. Iadarola, Beam-induced heat loads on the beam screens of the inner triplets for the HL-LHC, CERN-ACC-Note-2018-0009, CERN, Geneva, Switzerland, February 2018.
14. P. Costa Pinto et al, Amorphous carbon coating in SPS, In *Proc. 12th International Particle Accelerator Conference*, IPAC 2021, pp 3475-3478, Campinas, Brazil (May 2021).
15. R. Valizadeh et al, Low secondary electron yield engineered surface for electron cloud mitigation, Appl. Phys. Lett. 105, 231605 (2014).
16. M. Sitko et al, Towards the implementation of laser engineered surface structures for electron cloud mitigation, In *Proc. 9th International Particle Accelerator Conference*, IPAC 2018, pp 1220-1223, Vancouver, BC, Canada (May 2018).
17. V. Baglin, COLDEX: a tool to study cold surfaces in accelerators, In *Proc. 6th Electron-Cloud Workshop*, ECLOUD'18, pp 165-178, La Biodola, Italy (June 2018).
18. R. Salemme, Space charge compensation and electron cloud effects in modern high intensity proton accelerators, *PhD: Universita di Roma Sapienza*, *October 2016*, CERN-THESIS-2016-337.
19. F. Sanchez Galan et al, Optimising machine-experiment interventions in HL-LHC, In *Proc. 8th International Particle Accelerator Conference*, IPAC 2017, pp 3540-3543, Copenhagen, Denmark (May 2017).